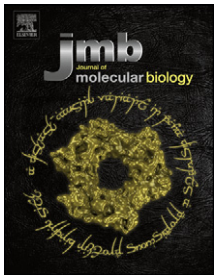

Multiple Weak Linear Motifs Enhance Recruitment and Processivity in SPOP-Mediated Substrate Ubiquitination

Wendy K. Pierce[1], Christy R. Grace[1], Jihun Lee[1], Amanda Nourse[2], Melissa R. Marzahn[1], Edmond R. Watson[1,3], Anthony A. High[4], Junmin Peng[1,4,5], Brenda A. Schulman[1,6] and Tanja Mittag[1]

1 - Department of Structural Biology, *St. Jude Children's Research Hospital, 262 Danny Thomas Place, Memphis, TN 38105, USA*
2 - Molecular Interactions Analysis Shared Resource, *St. Jude Children's Research Hospital, 262 Danny Thomas Place, Memphis, TN 38105, USA*
3 - Department of Microbiology, *Immunology, and Biochemistry, University of Tennessee Health Sciences Center, Memphis, TN 38105, USA*
4 - St. Jude Proteomics Facility, *St. Jude Children's Research Hospital, 262 Danny Thomas Place, Memphis, TN 38105, USA*
5 - Department of Developmental Neurobiology, *St. Jude Children's Research Hospital, 262 Danny Thomas Place, Memphis, TN 38105, USA*
6 - Howard Hughes Medical Institute, *St. Jude Children's Research Hospital, 262 Danny Thomas Place, Memphis, TN 38105, USA*

Correspondence to Tanja Mittag: *tanja.mittag@stjude.org*
http://dx.doi.org/10.1016/j.jmb.2015.10.002
Edited by P. Wright

Abstract

Primary sequence motifs, with millimolar affinities for binding partners, are abundant in disordered protein regions. In multivalent interactions, such weak linear motifs can cooperate to recruit binding partners via avidity effects. If linear motifs recruit modifying enzymes, optimal placement of weak motifs may regulate access to modification sites. Weak motifs may thus exert physiological relevance stronger than that suggested by their affinities, but molecular mechanisms of their function are still poorly understood. Herein, we use the N-terminal disordered region of the Hedgehog transcriptional regulator Gli3 ($Gli3^{1\text{-}90}$) to determine the role of weak motifs encoded in its primary sequence for the recruitment of its ubiquitin ligase $CRL3^{SPOP}$ and the subsequent effect on ubiquitination efficiency. The substrate adaptor SPOP binds linear motifs through its MATH (*m*eprin *a*nd *T*RAF *h*omology) domain and forms higher-order oligomers through its oligomerization domains, rendering SPOP multivalent for its substrates. Gli3 has multiple weak SPOP binding motifs. We map three such motifs in $Gli3^{1\text{-}90}$, the weakest of which has a millimolar dissociation constant. Multivalency of ligase and substrate for each other facilitates enhanced ligase recruitment and stimulates $Gli3^{1\text{-}90}$ ubiquitination in *in vitro* ubiquitination assays. We speculate that the weak motifs enable processivity through avidity effects and by providing steric access to lysine residues that are otherwise not prioritized for polyubiquitination. Weak motifs may generally be employed in multivalent systems to act as gatekeepers regulating post-translational modification.

Introduction

Intrinsically disordered and flexible protein regions contain an abundance of primary sequence motifs that function to recruit binding partners, direct modifying enzymes and rewire signaling networks [1–8]. Many of these linear motifs are only weakly conserved and may have affinities for their binding partners that are too weak to probe by high-throughput methods. This raises the question of how strong an individual interaction must be to have a physiological function. If multiple linear motifs in a protein interact with repeats of interaction domains in a binding partner, described as multivalent

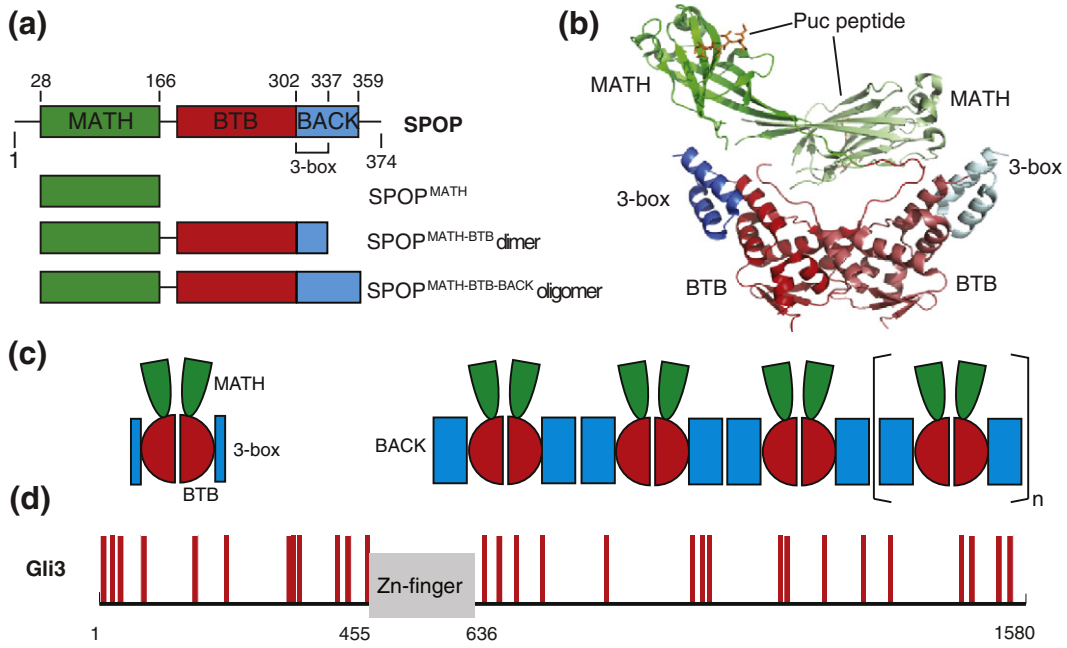

Fig. 1. Multivalency of Gli3 and SPOP. (a) Cartoon diagram of SPOP. SPOP contains a MATH domain for substrate recognition, a BTB domain for dimerization [32] and a BACK domain with an additional oligomerization function [16]. We used constructs encoding monomeric SPOP^{MATH} (28–166), dimeric SPOP$^{MATH-BTB}$ (28–337) [32] and higher-order oligomer-forming SPOP$^{MATH-BTB-BACK}$ (28–359) [16]. (b) Ribbon diagram of the asymmetric SPOP$^{MATH-BTB}$ dimer bound to two SB motif peptides, shown in orange in stick representation, PDB ID 3HQI [32]. One monomer in the ribbon diagram is colored more lightly. (c) Schematic of the domain structure of SPOP dimer (left) and SPOP oligomer (right). The linear SPOP oligomer schematic is based on the dimer structures of the BTB and BACK domains [33,32] and indicates the possibility for indefinite self-association. (d) Gli3 has a folded zinc finger (Zn finger) DNA-binding domain that encompasses residues 455–636; all other regions are predicted to be largely intrinsically disordered (see Fig. S1, Supplementary Material). By using the consensus SB sequence (Φ-π-S-S/T-S/T; Φ, nonpolar residue, π, polar residue) [32] and allowing for one mismatch, we predicted 29 weak consensus SB motifs, which are shown as red bars.

interactions, even weak individual interactions can contribute through avidity effects [9–14]. Such multivalent interactions may thus serve to increase the affinity and specificity of modular interactions [15]. In the context of substrate/enzyme interactions, multivalency can serve to regulate access to modification sites. Weak motifs may position an enzyme favorably relative to modification sites and thus contribute to the overall efficiency of the reaction to a degree higher than that expected from their affinities. In multi-turnover reactions, avidity effects have the potential to reduce substrate off-rates and may therefore serve to increase the processivity [16].

Many ubiquitin ligases recruit substrates by recognition of linear motifs (reviewed in Ref. [17]). The existence of multiple weak motifs in substrates has been attributed to precise regulation of substrate levels, for example, via the creation of switch-like dose–response curves [18,19]. Some ubiquitin ligases oligomerize and form dimers, tetramers or even higher-order oligomers [20–25,16]. Abolishing their oligomerization often results in a decrease in their ubiquitination activity [14,26,27]. The combination of an oligomeric ubiquitin ligase with a substrate with multiple weak motifs may create interesting opportunities for regulation.

Herein, we characterize the function of weak linear motifs in a substrate for its recruitment by the cullin3 RING ligase (CRL3) oligomeric substrate adaptor Speckle-type POZ protein (SPOP) [28–31]. SPOP recognizes primary sequence motifs with the consensus sequence Φ-π-S-S/T-S/T (Φ, nonpolar residue; π, polar residue) in its substrates and binds them in the substrate-binding groove of its MATH (*me*prin *a*nd *T*RAF *h*omology) domain (Fig. 1a and b) [32]. SPOP recruits CRL3 subunits through its 3-box [32] and dimerizes through its BTB (*B*ric à Brac, *T*ramtrack and *B*road complex) domain; crystal structures of these dimers are known (Fig. 1b) [32,16]. Recently, an additional oligomerization function has been assigned to the C-terminal BACK (*B*TB *a*nd *C*-terminal *K*elch) domain [16,33] (Fig. 1a). The presence of two oligomerization domains facilitates self-association into higher-order SPOP homo-oligomers [16] (Fig. 1c), rendering SPOP multivalent for substrates. The SPOP

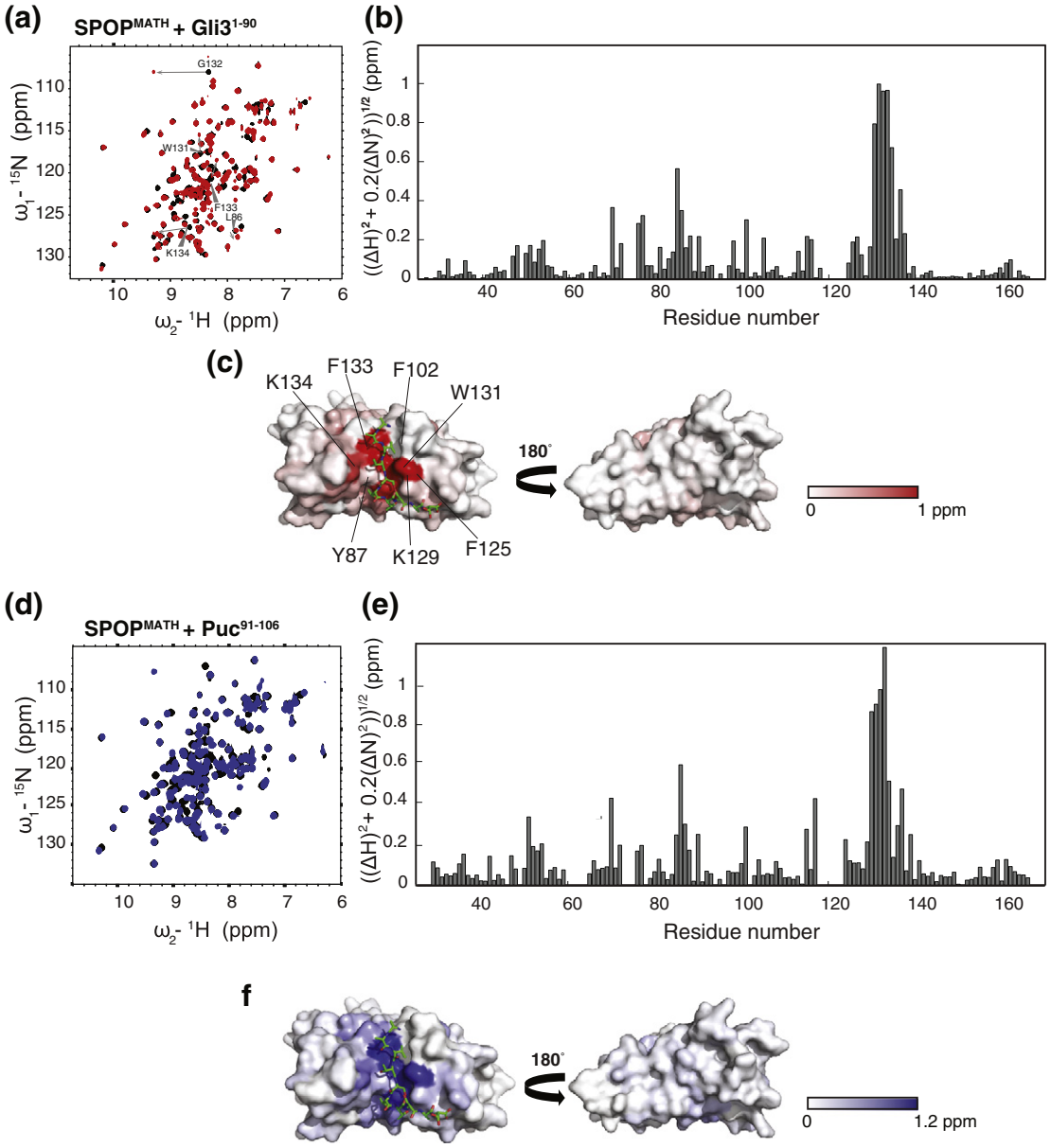

Fig. 2. Gli3$^{1\text{-}90}$ is recognized in the canonical MATH domain substrate-binding groove. (a and d) ^{15}N TROSY-HSQC spectra of free ^{15}N SPOP^{MATH} (black) and its complexes with (a) multivalent Gli3$^{1\text{-}90}$ (red) and (d) monovalent pPuc$^{91\text{-}106}$ (blue). (b and e) Combined ^{1}H and ^{15}N chemical shift perturbations of ^{15}N SPOP^{MATH} upon binding (b) Gli3$^{1\text{-}90}$ or (e) Puc$^{91\text{-}106}$ demonstrate the involvement of the same interface. (c and f) Chemical shift perturbations mapped onto the surface of SPOP^{MATH} in a color code from white to red [Gli3$^{1\text{-}90}$ (c)] or from white to blue [Puc$^{91\text{-}106}$ (f)] show that residues forming the canonical groove undergo the largest perturbations. Residues frequently mutated in prostate cancer cases are labeled in (c) [35].

substrates Gli2 and Gli3, which are transcriptional regulators of the Hedgehog signaling pathway, contain several regions that aid in their recognition by SPOP [34]. SPOP and SPOP substrates are thus multivalent for each other. Single strong binding motifs for monomeric ubiquitin ligases can efficiently target substrates for degradation [17]. The multivalency of SPOP/substrate pairs suggests an additional layer of regulation of substrate levels.

SPOP mutations have been recently identified in endometrial and prostate cancers [35–37] among others, and *SPOP* is the most frequently mutated gene in prostate cancer [35]. Most *SPOP* mutations are clustered in the substrate-binding groove and

abolish substrate binding [35,38,39]. Loss of SPOP expression occurs frequently in colorectal, gastric and prostate tumors [40]. Therefore, *SPOP* acts as a tumor suppressor under physiological conditions [41], and loss-of-function mutations or a redirection of SPOP activity to a different set of substrates serves to drive tumorigenesis [42,43]. Dissecting the mechanism of substrate recognition by SPOP is important to understand its normal function and role in pathogenesis.

In this study, we used biophysical techniques and functional assays to characterize the role of weak SPOP binding (SB) motifs in a disordered region of Gli3 for recruitment of SPOP and for $CRL3^{SPOP}$-mediated ubiquitination. We used nuclear magnetic resonance (NMR) spectroscopy, fluorescence anisotropy (FA) binding assays and analytical ultracentrifugation (AUC) to map SB motifs in a model multivalent substrate. We determined affinities to monomeric forms of SPOP by biolayer interferometry (BLI) and assessed how SPOP oligomerization affects recognition of the multivalent substrate. *In vitro* ubiquitination assays provided insight into the role of multivalency and the contribution of individual weak motifs for polyubiquitination. These studies provide understanding of the functional role of weak SB motifs in a multivalent interaction.

Results

To gain molecular insights into the biophysical mechanism of the multivalent interaction between Gli3 and SPOP, we first analyzed the primary sequence of Gli3 and predicted 29 SB motifs based on the known SB consensus motif sequence Φ-π-S-S/T-S/T [32], if we allowed for one mismatched position (Fig. 1d). These motifs are likely solvent accessible; apart from the folded zinc finger DNA-binding domain (residues 455–636 according to sequence alignment with Gli1 [44]), Gli3 is predicted to be largely intrinsically disordered (see Supplementary Fig. S1). The interaction of a highly multivalent substrate with oligomeric SPOP is likely complicated. To gain insight into this interaction, we characterized the interaction of the 90-residue N-terminal Gli3 fragment ($Gli3^{1\text{-}90}$), which we predicted to have four SB motifs, with monomeric, dimeric and oligomeric variants of SPOP. We determined the position and affinities of SB motifs and how they contribute to SPOP recruitment and Gli3 ubiquitination.

A multivalent Gli3 fragment binds to the MATH domain substrate-binding groove

The MATH domain of SPOP ($SPOP^{MATH}$) binds SB motifs in its substrate-binding groove across an antiparallel β-sheet (Fig. 1b) [32]. To investigate whether multivalent substrates bind to $SPOP^{MATH}$ via the groove alone or whether they have additional interactions with other regions of $SPOP^{MATH}$, we titrated $Gli3^{1\text{-}90}$ into ^{15}N-labeled $SPOP^{MATH}$ and followed perturbations of $SPOP^{MATH}$ amide resonances by NMR (Fig. 2a). Resonance assignments of the free and bound states of $SPOP^{MATH}$ (Supplementary Fig. S2) allowed us to calculate chemical shift perturbations (Fig. 2b). Strong perturbations were observed only for residues clustered around the canonical groove (Fig. 2c). Residues known to directly contact the SB motif in crystal structures of $SPOP^{MATH}$/motif complexes underwent the largest chemical shift perturbations. These perturbations were in slow exchange on the NMR timescale as observed by the progressive appearance of bound-state signals while the signals of the free state disappeared (Supplementary Fig. S3). Specifically, residues Y87, F102, F125, K129, W131, F133 and K134, which are mutated in prostate cancer [35], exhibited the largest perturbations. This result confirms the crucial role of these residues in recognizing substrates and supports previous findings that $SPOP^{MATH}$ mutants found in prostate cancer have substrate binding defects [38,39]. Binding of a peptide derived from the *Drosophila melanogaster* protein Puckered (pPuc; Ac^{91}-ENLACDEVTSTTSSST^{106}-NH_2), which contains one known strong SB motif, produced similar chemical shift perturbations (Fig. 2d–f). Additional perturbations mapping to the back of $SPOP^{MATH}$ were small and observed for binding of both $Gli3^{1\text{-}90}$ and pPuc and therefore likely do not indicate additional interactions but rather small conformational changes of $SPOP^{MATH}$ upon ligand binding. These findings confirm that multivalent $Gli3^{1\text{-}90}$ interacts with $SPOP^{MATH}$ via its canonical substrate-binding groove.

$Gli3^{1\text{-}90}$ is intrinsically disordered

To map the location of SB motifs in the $Gli3^{1\text{-}90}$ sequence (Fig. 3a), we used NMR spectroscopy and first assigned the $Gli3^{1\text{-}90}$ resonances (Fig. 3b) from spectra recorded at 5 °C, where maximum chemical shift dispersion was observed. NMR spectroscopy is a powerful method for characterizing the conformational and dynamic properties of intrinsically disordered proteins [45–47]. The narrow line widths and small $^1H^N$ chemical shift dispersion of the amide proton signals [48,49] showed that this region of Gli3 is disordered, in agreement with *in silico* predictions (see Supplementary Fig. S1) and previous reports [50].

^{1}H-^{15}N heteronuclear nuclear Overhauser enhancement (hetNOE) values, which provide information on fast protein dynamics and flexibility [51], were mostly negative when measured at 600 MHz

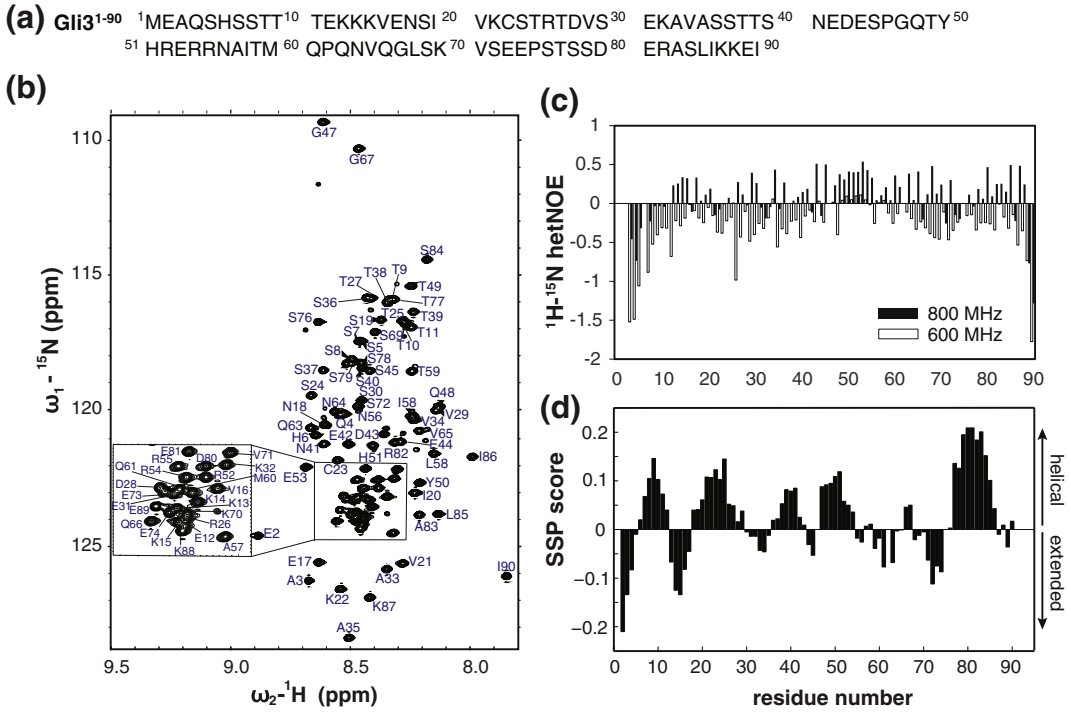

Fig. 3. Gli3[1-90] is intrinsically disordered. (a) Primary sequence of the Gli3[1-90] fragment. (b) ^{15}N HSQC spectrum with resonance assignments, Biological Magnetic Resonance Bank ID 26575. (c) ^{1}H-^{15}N hetNOE values at 25 °C and (d) secondary structure propensity (SSP) scores [53] calculated from C^{α} and C^{β} chemical shifts demonstrate that Gli3[1-90] is intrinsically disordered and samples transient structure.

and 25 °C and slightly positive at the center of the protein at 800 MHz (Fig. 3c). The modulation of the hetNOE by the location in the polypeptide chain and the relatively strong modulation by the field strength were expected for an intrinsically disordered protein and indicated that the protein was flexible with some motional restriction [52]. The region between residues 45 and 60, which exhibits the highest hetNOE values, also has transverse relaxation rates higher than those of the rest of the protein (Supplementary Fig. S4), suggesting the presence of transient interactions within this region.

Secondary structural propensities calculated from C^{α} and C^{β} chemical shifts [53] demonstrated the presence of stretches with ≥10% helicity for Gli3[6-12], Gli3[18-29], Gli3[36-43], and Gli3[47-54] and up to 20% helicity for Gli3[77-86]. The rest of the protein had a propensity to sample extended conformations (Fig. 3d). The disordered nature of Gli3[1-90] likely provides accessibility for binding partners, including SPOP.

Gli3[1-90] has three weak SB motifs

In mapping the location of SB motifs in Gli3[1-90], we wanted to avoid bias toward the discovery of motifs with the known consensus motif because weak binding motifs with distinct sequences may be able to contribute to the multivalent interaction with SPOP. We therefore implemented a three-pronged approach consisting of (1) a titration of SPOP[MATH] into ^{15}N-labeled Gli3[1-90], (2) division of the candidate sequences into 15-residue-long peptides and assessment of their ability to compete with pPuc for SPOP[MATH] binding in a secondary FA binding assay and (3) a tertiary NMR binding assay to monitor binding of peptides to ^{15}N SPOP[MATH]. This combined approach allowed the identification of SB motifs and the exclusion of false-positive candidate motifs.

First, we titrated deuterated SPOP[MATH] into ^{15}N-labeled Gli3[1-90] up to a 3.2-fold molar ratio and assigned the resonances of the complex. Resonances in three regions, at the N-terminus, in the middle and close to the C-terminus of the protein, were not assignable. We monitored chemical shift perturbations in ^{1}H-^{15}N heteronuclear single quantum coherence (HSQC) spectra. As expected, many resonances, in particular, serine and threonine resonances (see Supplementary Fig. S5), experienced chemical shift perturbations because SB motifs are serine/threonine rich. Chemical shift perturbations were largest around the regions that could not be assigned in the complex, suggesting that these regions contained SB motifs (Fig. 4a).

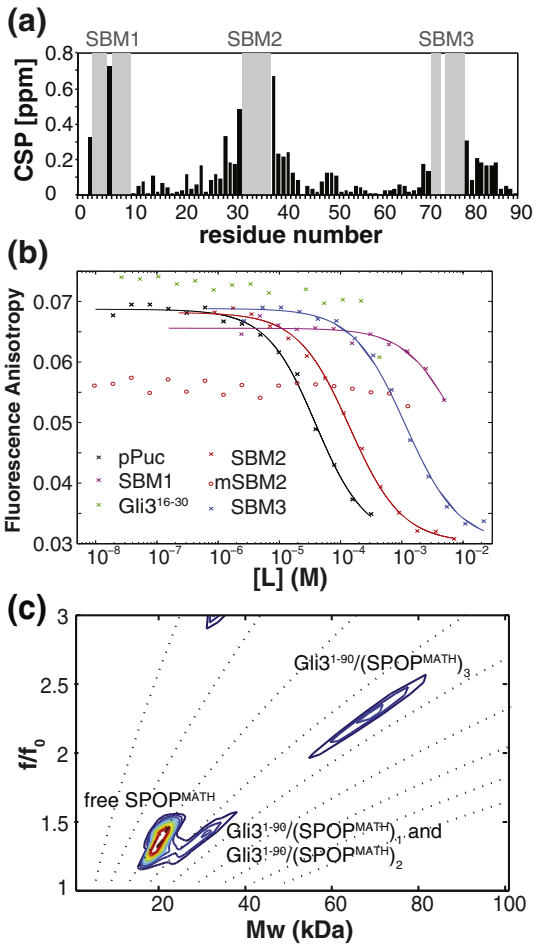

Fig. 4. Gli3$^{1\text{-}90}$ can bind up to three SPOP^{MATH} molecules. (a) Chemical shift perturbations $[(\Delta H^2 + 0.2\Delta N^2)^{1/2}]$ for Gli3$^{1\text{-}90}$ upon SPOP^{MATH} binding (at a molar ratio of 1:3.2). Residues shown in grey could not be assigned in the complex spectrum. These regions correspond to the three SB motifs in Gli3$^{1\text{-}90}$. (b) Peptides containing candidate SB motifs compete with fluorescein-Puc$^{91\text{-}106}$ for binding to SPOP^{MATH} in an FA competition assay. [L] is the peptide concentration. Continuous lines are non-linear least-squares fits to a complete competitive binding model [54]. See Table 1 for K_D values. (c) Two-dimensional size-and-shape distribution analysis of SV AUC data of a Gli3$^{1\text{-}90}$/SPOP^{MATH} mixture. Contour plots of $c(M,f/f_0)$ of the transformed velocity data with 0 fringes/S (white) to maximum-value fringes/S (red), with increasing color temperature indicating higher values are presented. The dotted lines are lines of constant *s*-value.

We then generated 15-residue-long peptides covering these regions and used an FA competition assay [54] to test their ability to bind to the SPOP-^{MATH} groove by competing with fluorescein-labeled pPuc (F-pPuc). The assay yielded a dissociation constant (K_D) of 7.7 μM for pPuc (Table 1), which is in good agreement with previous data [32]. Peptides encompassing regions Gli3$^{1\text{-}15}$, Gli3$^{30\text{-}45}$, and Gli3$^{70\text{-}84}$ competed with pPuc for binding to SPOP^{MATH} and are referred to as SBM1, SBM2, and SBM3, respectively, hereafter (Fig. 4b and Table 1). We further confirmed the interaction of some of these peptides by monitoring chemical shift perturbations in ^{1}H-^{15}N HSQC spectra of ^{15}N SPOP^{MATH}. The peptides elicited similar perturbation patterns, but perturbations were weaker than those for pPuc or Gli3$^{1\text{-}90}$, suggesting that individual motifs had weak binding affinities (see Supplementary Fig. S6).

The binding affinities of SBM2 and SBM3 to SPOP^{MATH} were weak, 80 μM and 560 μM, respectively (Table 1). As expected, mutation of the Ser/Thr-rich region in SBM2 to a generic disordered sequence (VASSTTS to VAGGSGS, previously used by Zhuang *et al.* to abolish substrate binding [32]) decreased binding to below the detection limit of the assay. Although we were able to monitor the binding to SBM1 effectively by NMR, we estimated from FA that its K_D was as high as ~4 mM. SBM1 lacks the hydrophobic residue at the motif N-terminus, likely accounting for its weak affinity. The order in which the individual motifs lost signal intensity in NMR titrations was consistent with the relative motif affinities measured for individual peptides by FA competition assays, indicating that transient structure in Gli3$^{1\text{-}90}$ did not alter the overall order of SB motif affinities (Supplementary Fig. 7).

The regions N- and C-terminal to SBM2 showed chemical shift perturbations as well, and thus, we tested peptides Gli3$^{16\text{-}30}$ and Gli3$^{41\text{-}59}$; neither peptide bound to SPOP^{MATH} in the FA assay (Table 1 and Fig. 4b). Gli3$^{16\text{-}30}$ does not contain a conventional SB motif; it contains a cysteine in place of the serine that was previously suggested to be invariable (VKCST instead of Φ-π-S-S/T-S/T) [32]. We speculated that this sequence might bind SPOP-^{MATH} but did not observe consistent binding by FA or NMR (Fig. 4b and Supplementary Fig. S6). Gli3$^{41\text{-}59}$ does not contain an SB-motif-like sequence. In the unbound state, this region of Gli3$^{1\text{-}90}$ has the highest hetNOE and R_2 values (Fig. 3c and Supplementary Fig. S4), and therefore, perturbation of its resonances may reflect a change in intramolecular interactions within Gli3$^{1\text{-}90}$ rather than intermolecular interactions with SPOP^{MATH} [55,56].

Together, these NMR and FA binding experiments show that we have identified three specific SB motifs in the N-terminus of Gli3. Among mammals, the entire N-terminus of Gli3 is highly conserved, while among vertebrates, the sequence similarity in the N-terminus is highest within the SB motifs (Supplementary Fig. S8), supporting the hypothesis that these motifs play a role in recruiting CRL3^{SPOP}.

Gli3$^{1\text{-}90}$ can simultaneously bind up to three MATH domain molecules

To derive the stoichiometry of binding, we used sedimentation velocity (SV) AUC in combination with two-dimensional size-and-shape distribution

Table 1. Peptide affinities to SPOP^{MATH}

Motif	Residue no.	Sequence	K_D (μM)[a]
pPuc	91–106	Ac-ENLACDEVTSTTSSST-NH_2	7.7 ± 0.2
SBM1	1–15	Ac-MEAQSHSSTTTEKK-NH_2	~4100
Gli3$^{16–30}$	16–30	Ac-VENSIVKCSTRTDVS-NH_2	nb[b]
SBM2	31–45	Ac-EKAVASSTTSNEDES-NH_2	80 ± 3
mSBM2	31–45	Ac-EKAVAGGSGSNEDES-NH_2	nb[b]
SBM3	71–84	Ac-KVSEEPSTSSDERA-NH_2	560 ± 30
Gli3$^{41-59}$	41–59	Ac-NEDESPGQTYHRERRNAIT-NH_2	nb[b]

[a] Errors represent standard errors from triplicate experiments from FA competition experiments.
[b] No binding detected.

analysis, which allows the determination of accurate molecular weights of several species with different frictional coefficients in a complex mixture [57]. In the presence of an excess of SPOP^{MATH}, up to three MATH domain molecules were able to bind to one Gli3$^{1-90}$ molecule (Fig. 4c). Furthermore, we observed both free SPOP^{MATH} and a signal at higher molecular weights in the f/f_0 value range from 1.2 to 1.6. We interpreted the latter to reflect a mixture of different 1:1 and 1:2 complexes, all likely having similar average molecular shapes and sizes. The 1:3 complex is easily distinguishable from the other signals because its larger M_w is combined with a large f/f_0 value of 2–2.5, which we attribute to an extended and possibly rigid shape. SV analysis of two dilutions of the complex showed reduction of the fractional population of the largest complex as expected and confirms that the data are self-consistent (Supplementary Fig. S9). These data support the notion that Gli3$^{1-90}$ can interact with one SPOP^{MATH} molecule through each of its three SB motifs, demonstrating that the motifs are accessible simultaneously.

Do SPOP dimers exhibit cooperative substrate binding?

Next, we explored whether the interaction of dimeric SPOP with substrates was dominated by avidity or cooperativity effects. We expected to find avidity effects in the SPOP/Gli3$^{1-90}$ interaction; that is, the first SB motif/MATH interaction would result in an increased local concentration of additional interaction partners and thus enhance binding. However, the binding of ligands to oligomeric proteins is sometimes cooperative; that is, it depends on the number of ligands already bound [58–60]. A monovalent ligand cannot exhibit avidity toward dimeric SPOP and can therefore be used to probe for cooperativity.

We used a direct FA binding assay in which we titrated either the SPOP^{MATH} domain or the SPOP$^{MATH-BTB}$ dimer into the fluorescently labeled Puc peptide. Both interactions yielded the same K_D of ~6 μM within error (Fig. 5). It is unlikely that the K_D for the second MATH domain becomes too large to measure once the first MATH domain is bound because a crystal structure of the SPOP dimer with two bound pPuc peptides exists [32] (see Fig. 1b). Therefore, the affinity of one MATH domain in the SPOP dimer is independent of the association state of the other MATH domain. We conclude that the SPOP dimer does not exhibit macroscopic cooperativity toward monovalent substrates. Avidity effects may instead play a role in its interactions with multivalent substrates.

Multivalent interactions afford avidity

To test for avidity effects, we determined the apparent affinities of SPOP constructs with increasing multivalency, utilizing monomeric, dimeric and higher-order oligomeric SPOP, to Gli3$^{1-90}$. Higher-order oligomeric SPOP accesses a distribution of different oligomers depending on the protein concentration, though the dimer is always the predominant species (Marzahn and Mittag, unpublished results). We used a BLI assay in which we immobilized His-tagged Gli3$^{1-90}$ on the sensor and

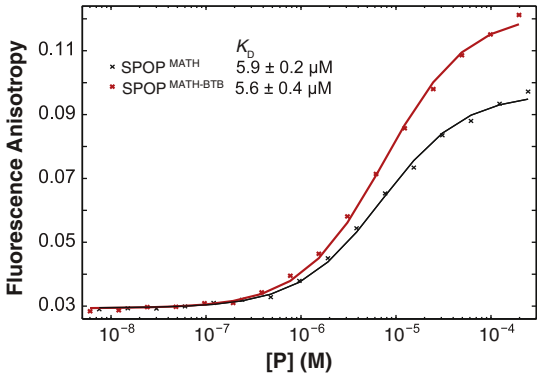

Fig. 5. SPOP dimer binds monovalent substrate without cooperativity. Direct FA binding data for monomeric SPOP^{MATH} (black) and dimeric SPOP$^{MATH-BTB}$ (red) to monovalent pPuc$^{91-106}$ is shown. [P] indicates the protein concentration.

Table 2. $Gli3^{1-90}$ affinities to SPOP constructs of different association state from kinetic fits of BLI data

SPOP construct	Association state	K_D (μM)[a]
$SPOP^{MATH}$	Monomer	21 ± 2
$SPOP^{MATH-BTB}$	Dimer	28 ± 6
$SPOP^{MATH-BTB-BACK}$	Higher-order oligomer	1.5 ± 0.1

[a] Errors represent standard errors from triplicate experiments from BLI.

monitored binding of the three SPOP constructs to it. Their concentrations were normalized to the number of protomers in solution; that is, solutions of monomeric, dimeric and oligomeric SPOP at the same concentration contained the same number of binding sites for SB motifs.

For $SPOP^{MATH}$, we obtained a K_D of 21 μM (Table 2 and Supplementary Fig. S10). The increased apparent affinity, when compared with the highest microscopic affinity (80 μM for SBM2; Fig. 4b and Table 1), may be caused by (i) the high local concentration of motifs and therefore an increased probability for a MATH domain molecule to rebind after its release, (ii) an entropic advantage because of a greater number of different bound states in a multivalent substrate or (iii) modifications of the affinities from flanking sequences outside of the core binding SB motifs (e.g., through long-range electrostatic interactions).

With dimeric $SPOP^{MATH-BTB}$, we do not see a significant change in the affinity compared to the monomeric $SPOP^{MATH}$. While we had expected an increased affinity due to engagement of two SB motifs via the two MATH domains, these data indicate that the SB motifs in $Gli3^{1-90}$ are not adequately spaced for avidity to the SPOP dimer. In contrast, the higher-order oligomer-forming $SPOP^{MATH-BTB-BACK}$ exhibited increased binding to $Gli3^{1-90}$ with a K_D of 1.5 μM (Table 2). These data demonstrate that multivalency of both proteins for each other leads to an affinity increase due to avidity effects.

Contribution of weak SB motifs to ubiquitination

As we observed increased substrate binding by oligomeric SPOP, we wondered whether this would also lead to enhanced $CRL3^{SPOP}$-mediated ubiquitination activity. We utilized His-$Gli3^{1-90}$ in standard *in vitro* ubiquitination assays with recombinant substrate, ubiquitin, E1, E2 and neddylated $CRL3^{SPOP}$ [32]. Transfer of ubiquitin moieties onto lysine residues of His-$Gli3^{1-90}$ were monitored by Western blot against the His-tag. A mixture of multi-monoubiquitinated or polyubiquitinated species resulted in a regular laddering appearance (Fig. 6a and b and Supplementary Fig. S11). We compared $CRL3^{SPOP}$ activity in the context of dimeric $SPOP^{MATH-BTB}$ *versus* oligomeric $SPOP^{MATH-BTB-BACK}$. We observed efficient ubiquitination after a 20-min reaction for oligomeric SPOP but smaller ubiquitinated species with dimeric SPOP (Fig. 6a). These results are in agreement with previously reported enhancement of ubiquitination efficiency upon SPOP dimerization [32] and oligomerization [16]. Together with our analysis of substrate binding, the data suggest that the multivalency of oligomeric SPOP and $Gli3^{1-90}$ for each other enhances recruitment of the substrate, thereby enhancing ubiquitination efficiency.

We observed a range of affinities for SB motif binding to SPOP and therefore postulated that the highly conserved motifs, even though weak, would play a distinct functional role. To test this hypothesis, we generated mutant $Gli3^{1-90}$ constructs that carried inactivating mutations [32] in one, two or all three SB motifs. Strikingly, the mutation of SBM1, which had the weakest binding affinity, resulted in a substantial attenuation of ubiquitination (Fig. 6b). Mutation of SBM2, which had the strongest binding affinity and was expected to essentially abolish the recruitment of SPOP, only had a moderate effect on ubiquitination levels (Fig. 6b). In general, combinations of mutations led to increasing loss of ubiquitination. Interestingly, a $Gli3^{1-90}$ mutant that carried only SBM1 sustained relatively efficient ubiquitination. These results demonstrate that even weak motifs in $Gli3^{1-90}$ contribute to ubiquitination by $CRL3^{SPOP}$. Reducing the multivalency, either by restricting the SPOP oligomerization state to dimers or by inactivating SB motifs in $Gli3^{1-90}$ reduced the overall ubiquitination efficiency.

Several studies have shown the importance of an optimal placement of acceptor lysines relative to the catalytic cysteine in ubiquitin ligases [61–64]. We speculated that the unexpected loss of ubiquitination in the SBM1 mutant, as well as the lesser sensitivity of the SBM2 mutation, reflected the accessibility of modifiable lysine residues in $Gli3^{1-90}$. We characterized the lysine residues that were ubiquitinated in wild-type (wt) $Gli3^{1-90}$ by using tryptic digestion and liquid chromatography–tandem mass spectrometry (LC-MS/MS) analysis of reaction mixtures and identified five ubiquitinated lysine residues, K15, K22, K32, K70 and K87 (Fig. 6c for summary and Supplementary Fig. S12). We observed ubiquitination of the same lysine residues for all mutants we tested, which included mSBM1, mSBM2 and mSBM23. While these experiments did not inform on the extent of ubiquitination at individual lysine residues, the results showed that not all SB motifs needed to be present simultaneously to provide access for lysine modification.

To further characterize whether the ubiquitination defect in some of the Gli3 mutants was a result of the modification of fewer lysine residues or less efficient building of polyubiquitin chains on all modifiable lysines, we carried out ubiquitination reactions with a lysine-less ubiquitin mutant (Ub noK, in which all

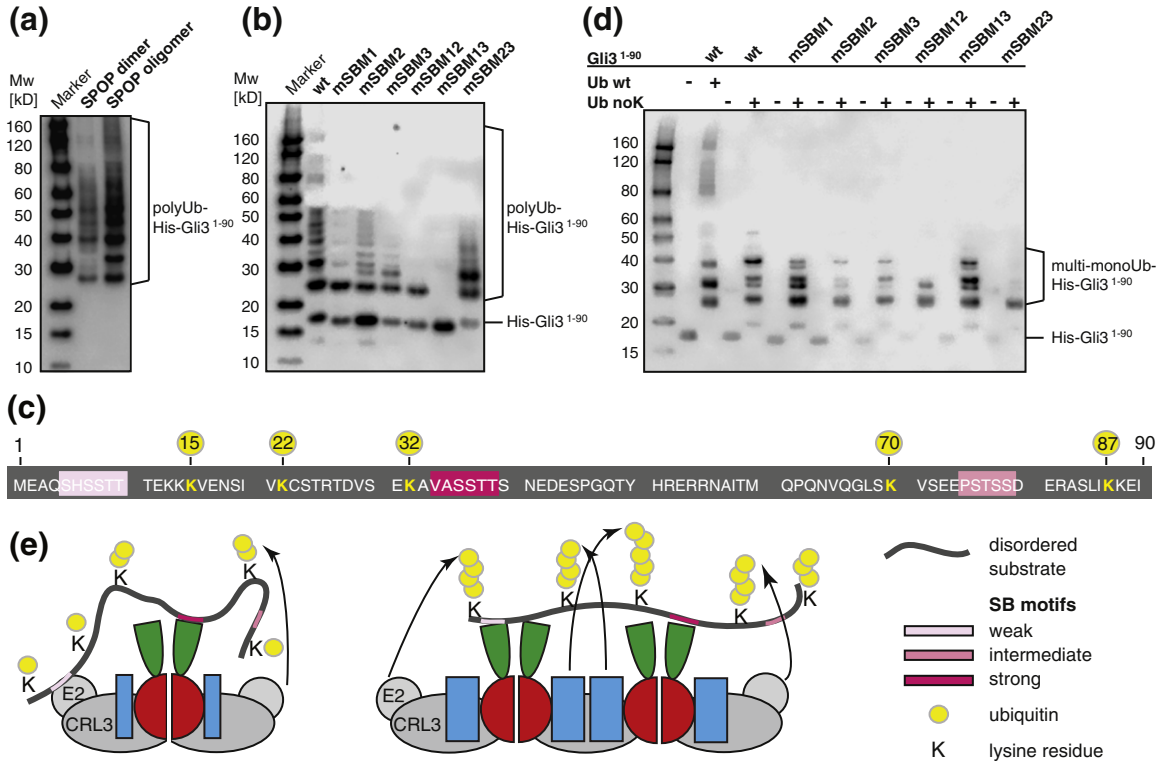

Fig. 6. Weak SB motifs stimulate CRL3^{SPOP}-mediated *in vitro* ubiquitination of Gli3$^{1-90}$. (a) Western blot showing *in vitro* ubiquitination of His-Gli3$^{1-90}$ by neddylated CRL3^{SPOP} with dimeric SPOP$^{MATH-BTB}$ or oligomeric SPOP$^{MATH-BTB-BACK}$. His-Gli3$^{1-90}$ is detected with an anti-6x-His antibody. (b and d) Western blot showing *in vitro* ubiquitination of wt and mutant His-Gli3$^{1-90}$ substrates by neddylated CRL3^{SPOP} with oligomeric SPOP$^{MATH-BTB-BACK}$ with (b) wt ubiquitin or (d) a lysine-less ubiquitin variant (Ub noK), which sustains only monoubiquitination on multiple lysines. mSBM1, mSBM2, mSBM3 and combinations refer to inactivating mutations of the three SB motifs. (c) Schematic representation of ubiquitin-modified lysine residues (yellow) in wt Gli3$^{1-90}$ substrate. (e) We present a model proposing the role of weak SB motifs and SPOP oligomerization in substrate recruitment and polyubiquitination. Dimeric SPOP recruits substrates with lower affinity and may not provide suitable steric access to lysine residues on growing polyubiquitin chains. In contrast, oligomeric CRL3^{SPOP} (a tetramer is shown for clarity) mediates enhanced recruitment via avidity effects and effective polyubiquitination through sterically favorable positioning relative to multiple catalytic centers in the oligomeric CRL3. SB motifs are depicted as pink bars, and the color saturation decreases for weaker motifs. Additional CRL3 components are not depicted for clarity.

lysines are replaced with arginines). Ub noK does not support building of polyubiquitin chains but supports monoubiquitination at individual lysine residues. The reactions were carried out for 1 h with higher E1 concentrations to reach an endpoint that showed the maximum number of modifiable lysine residues. We observed up to five modified lysine residues on wt Gli3$^{1-90}$ (Fig. 6d), in agreement with the LC-MS/MS results. Mutating one SB motif had only minor effects, with substrates still containing approximately four ubiquitinated lysines, although the ubiquitination patterns varied slightly among mutants, as observed by the bands on the Western blot (Fig. 6d). Most Gli3$^{1-90}$ mutants with less than two SB motifs were ubiquitinated on fewer lysines. The mSBM13 mutant, containing the highest-affinity SBM2 motif, however, sustained ubiquitination on four lysine residues. The mSBM23 mutant, which contains only the weakest affinity SBM1 motif, was only modified on approximately one to two lysines. In contrast, this mutant was highly ubiquitinated with wt ubiquitin (Fig. 6b). Therefore, the weakest motif, SBM1, is required to promote efficient polyubiquitination of Gli3$^{1-90}$.

These results demonstrate that monoubiquitination is sustainable by the highest-affinity motif but that the presence of additional motifs, even if they have millimolar affinities, drives effective polyubiquitination, likely by enabling processivity of the ligase.

Discussion

Herein, we have demonstrated that weak linear binding motifs can strengthen protein/protein interactions and mediate function in multivalent systems,

even if their dissociation constants are in the millimolar range. We identified three SB motifs in the intrinsically disordered N-terminus of Gli3; the strongest motif had a microscopic K_D of 80 μM, while the others were in the range from hundreds of micromolars to millimolars (Table 1). Together, they mediated binding to oligomeric SPOP at a low micromolar affinity (Table 2). These observations support a model in which dual multivalency, that is, multivalency of each binding partner for the other, enhances binding through avidity effects, where the resulting binding is stronger than each individual interaction. The likely mechanism is the increase of the local concentration of a second pair of binding partners once the first interaction is made [11,9]. Interestingly, SPOP dimerization did not enhance binding of $Gli3^{1\text{-}90}$ compared to the SPOP monomer (Table 2). Although $Gli3^{1\text{-}90}$ supports binding of three MATH domain molecules simultaneously (Fig. 4c), the SB motifs may not be optimally spaced for avidity with SPOP dimers.

In addition to the role of multivalency in substrate recruitment, multivalency was required for the full activity in an *in vitro* ubiquitination assay. *Either* inactivating SPOP's ability to oligomerize or inactivating the weakest $Gli3^{1\text{-}90}$ SB motif led to a defect in $Gli3^{1\text{-}90}$ ubiquitination. However, all lysine residues that were ubiquitinated in wt $Gli3^{1\text{-}90}$ were also available for modification in the mutants. Therefore, we propose that the defect stems from a lack of processivity of $CRL3^{SPOP}$, caused by the following two mechanisms: (1) mutant substrates with lower affinities due to a lack of avidity with SPOP experience higher off-rates from the ligase and consequently lower ubiquitination rates and (2) binding to three SB motifs mediates sterically favorable placement of multiple catalytic ligase centers to accommodate the changing distances in a growing ubiquitin chain. We conclude that SBM1, the weakest binding motif, plays a particularly important role in positioning the substrate relative to catalytic cysteines because of its disproportionate effect on polyubiquitination. For mSBM23, the mutant that only harbors SBM1, monoubiquitination is reduced to one site (Fig. 6d) but polyubiquitination of this mutant is more effective than that for others (Fig. 6b). We speculate that SPOP oligomerization has a similar functional impact as adding additional weak SB motifs to a substrate, that is, that multivalency of the substrate and $CRL3^{SPOP}$ for each other is decisive for processivity and thus polyubiquitination.

Our data suggest that even motifs that vary substantially from the consensus sequence support substrate ubiquitination, warranting a broader search for substrates than possible by sequence comparison with known motifs. How SPOP achieves substrate specificity despite its ability to recognize very weak motifs remains to be investigated.

Previous work showed that $CRL3^{SPOP}$-mediated *in vitro* ubiquitination of Puc is driven by its strongest motif and that contribution of the two weaker motifs is negligible [32]. The inactivity of the weak motifs in Puc might be explained by the use of dimeric SPOP in the previous report and the concurrent lack of dual multivalency and avidity. The absolute affinity of the motifs in Puc *versus* $Gli3^{1\text{-}90}$ also differs; the strong Puc motif is the strongest known SB motif with a K_D of ~4 μM and may therefore dominate SPOP recruitment, even in the absence of SPOP oligomerization. We speculate that weak motifs are only functional in the context of highly multivalent substrates. They may serve to enable ultrasensitive substrate concentration/degradation responses [65]. In contrast, we speculate that substrates with few strong motifs are polyubiquitinated constitutively because they are readily recruited to the ligase.

In addition to avidity, cooperativity is a possible mechanism for enhancing binding to oligomeric proteins. As cooperativity requires concerted changes of conformation or dynamics within the oligomeric protein upon binding the first binding partner, avidity may be simpler to realize through the use of a disordered protein with multiple motifs. The ubiquitous nature of disordered regions and linear motifs within them may attest to this fact.

Extrapolating from the three SB motifs we have mapped in $Gli3^{1\text{-}90}$, assuming constant density of SB motifs in all disordered regions, we would expect up to 46 SB motifs in full-length Gli3. Obviously, this deduction may not reflect reality; the density of SB motifs may be higher in the N-terminus. Nevertheless, previous reports have mapped several SPOP-recruiting regions in different parts of Gli3 [34]. In fact, a high density of short linear motifs has been reported in disordered regions of some proteins as a functional benefit and is therefore not unexpected [66,67]. We expect that the presence of many weak motifs in combination with higher-order oligomerization of a binding partner enables tight regulation of the interaction. In fact, higher-order oligomerization of enzymes and the assembly of signaling machines are emerging as a new paradigm of signal transduction and are thought to mediate signal amplification, ultrasensitive responses, noise reduction and exquisite temporal and spatial signaling control (reviewed in Ref. [65]).

The dysregulation of the Gli3/SPOP interaction may be expected to affect Gli3 turnover. Mutations of S8 and S36 in Gli3 have been reported in cancers[†] [68,69] and may negatively affect SPOP recruitment because these serines are located in motifs characterized herein, SBM1 and SBM2 (Fig. 3a and b). SB motifs in other parts of Gli3 not characterized here may be affected similarly. Though mutation of several SB motifs in a substrate is an unlikely event, single point mutations in SPOP can greatly affect its multivalency. Indeed, mutations of BTB and

BACK domain interface residues that may affect SPOP's ability to oligomerize have been found in sequencing efforts of melanoma and uterine cancers[1] [68–71]. Mutations in the substrate-binding groove of the MATH domain are usually not accompanied by loss of heterozygosity [35]. In the presence of wt and mutant SPOP, SPOP hetero-oligomers with reduced multivalency must form because wt protomers are able to bind SB motifs while mutant protomers are not. While levels of substrates with many weak linear motifs may be exquisitely regulated in healthy cells, in the presence of wt/mutant SPOP hetero-oligomers, their turnover is likely impacted more strongly than that of substrates with individual strong motifs. Therefore, SPOP mutations may affect subsets of substrates, potentially changing substrate selectivity [43].

Despite tremendous progress in our understanding of individual systems, the rules of lysine selection by E2/E3/ubiquitin-like modifier trios [62] and for achieving monoubiquitination and polyubiquitination [72–74] are still poorly understood in general. The presence of multiple linear motifs has the potential to drive lysine selection and determine the extent of polyubiquitination as we suggest here; altering the number of "active" linear motifs by post-translational modification or conformational changes thus adds an additional possible regulatory layer. If the extent of ligase oligomerization is regulated as well, as has been suggested previously [16], astounding combinatorial possibilities for substrate selection ensue.

Weak linear motifs, when appearing in multiples in disordered protein regions, have the potential for extensive function. A deeper understanding of the regulation of $CRL3^{SPOP}$ activity toward multivalent substrates will ultimately provide insight into protein homeostasis in health and disease.

Methods

Constructs and cell cultures

The coding sequence for a Gli3 fragment spanning residues 1–90 ($Gli3^{1-90}$) was cloned into a pET28a vector and overexpressed in *Escherichia coli* BL21 (DE3) RIPL cells (Agilent Technologies) in LB medium at 37°C with shaking at 280 rpm, and expression was induced with 1 mM isopropyl β-D-1-thiogalactopyranoside. The expression of GST-$SPOP^{MATH}$ (residues 28–166) and dimeric His-MBP-$SPOP^{MATH-BTB}$ (residues 28–337) has been previously described [32]. Briefly, these constructs, GST-$SPOP^{MATH-BTB}$ and His-SUMO-$SPOP^{MATH-BTB-BACK}$ (residues 28–359), were expressed in BL21 GOLD cells (Agilent Technologies) in LB medium for unlabeled samples or M9 minimal medium supplemented with ^{15}N NH_4Cl and/or ^{13}C glucose, depending on the desired labeling scheme. Expression was induced with 0.6 mM isopropyl β-D-1-thiogalactopyranoside at OD_{600} ~0.6 at 18°C with shaking at 280 rpm overnight. Cells were harvested by centrifugation and lysed with a microfluidizer (Microfluidics).

Protein purification

His-tagged $Gli3^{1-90}$ was purified using 20 mL Ni-NTA resin in buffer containing 50 mM Tris (pH 8), 300 mM NaCl, 30 mM imidazole and 2 mM β-mercaptoethanol (β-ME) and was eluted in buffer containing 25 mM Tris (pH 8), 300 mM NaCl, 300 mM imidazole and 2 mM β-ME. The resulting protein was cleaved with tobacco etch virus (TEV) protease under dialysis at 4°C overnight against 25 mM Tris (pH 8), 500 mM NaCl, 20 mM imidazole and 5 mM β-ME or the His tag was left attached for BLI and ubiquitination assays. The cleaved product was passed through Ni-NTA resin to remove uncleaved protein and TEV protease.

GST-$SPOP^{MATH}$, GST-$SPOP^{MATH-BTB}$ and GST-$SPOP^{MATH-BTB-BACK}$ were purified using glutathione-Sepharose in PBS (pH 7.3) and 5 mM DTT and were eluted with PBS (pH 7.3), 5 mM DTT and 10 mM reduced L-glutathione. His-MBP-$SPOP^{MATH-BTB}$ was purified on 20 mL of Ni-NTA resin, followed by simultaneous TEV cleavage and dialysis at 4°C into PBS (pH 7.6) and 5 mM DTT overnight. Ion-exchange chromatography to separate the cleaved tags from SPOP was performed on a 5-mL HiTrap SP column (for $SPOP^{MATH}$; GE Healthcare) or on a 5-mL HiTrap Q column (for $SPOP^{MATH-BTB}$), using a gradient from 0 to 700 mM NaCl.

All proteins were further purified by size-exclusion chromatography on a HiLoad 16/60 Superdex 75 or 200 gel-filtration column in 20 mM Tris (pH 7.6), 150 mM NaCl and 5 mM DTT or in NMR buffer (see below).

The protein purity was at least 95%, as shown by SDS-PAGE and SV AUC (see Supplementary Fig. S13). Protein identities were confirmed by both top–down and bottom–up mass spectrometry.

Peptide synthesis

Fifteen residue peptides encompassing the SB motifs were synthesized through the Hartwell Center, St. Jude Children's Research Hospital, or were purchased from GenScript. Each peptide allows for approximately four residues preceding and following the consensus sequence. All peptides were modified by N-terminal acetylation and C-terminal amidation.

Fluorescence anisotropy

An N-terminally fluorescently labeled Puc peptide (F-pPuc) with sequence ^{91}Ac-ENLACDEVTSTTSSST-NH_2^{107} was purchased from GenScript. For direct FA binding assays, increasing concentrations of $SPOP^{MATH}$ and $SPOP^{MATH-BTB}$ were titrated into 40 nM F-pPuc in a buffer containing 20 mM Tris (pH 7.4), 150 mM NaCl, 1% bovine serum albumin (Sigma) and 0.01% Triton X-100, and the FA was monitored with an EnVision multilabel plate reader (PerkinElmer) at 25°C. For competition experiments, increasing concentrations of each peptide were individually titrated into a mixture of 6 μM $SPOP^{MATH}$

and 40 nM F-pPuc and the FA was monitored. Analysis was performed as described previously [54].

NMR spectroscopy

NMR data were acquired on Bruker Avance 600 and 800 MHz spectrometers equipped with TCI triple-resonance cryogenic probes and pulsed-field gradient units. All samples were prepared in an NMR buffer consisting of 50 mM NaCl, 2.7 mM KCl, 10 mM Na_2HPO_4, 1.76 mM KH_2PO_4 and 5 mM DTT (pH 6.0) at 5°C. For assignment, a sample of 1.5 mM ^{15}N Gli3$^{1\text{-}90}$ was used to acquire standard triple-resonance backbone assignment experiments. These included a HNCACB and CBCA(CO)NH with 16 scans and 8 scans, respectively, and 1024 (^{1}H) × 28 (^{15}N) × 60 (^{13}C) complex data points, with 10 ppm, 22 ppm and 70 ppm for ^{1}H, ^{15}N and ^{13}C sweep widths, respectively. Both HNCO and HN(CA)CO were acquired with 8 scans, 1024 (^{1}H) × 20 (^{15}N) × 64 (^{13}C) complex data points, with 10 ppm, 22 ppm and 22 ppm for ^{1}H, ^{15}N and ^{13}C sweep widths, respectively.

Initial SPOP^{MATH} assignments were obtained from the authors who solved the solution NMR structure of SPOP-^{MATH} (PDB ID: 2CR2) and the assignments were confirmed using three-dimensional HNCA [1024 (^{1}H) × 24 (^{15}N) × 40 (^{13}C) complex data points, with 14 ppm (^{1}H), 32 ppm (^{15}N) and 32 ppm (^{13}C) sweep widths] and CBCA(CO)NH [1024 (^{1}H) × 24 (^{15}N) × 44 (^{13}C) complex data points, with 14 ppm (^{1}H), 32 ppm (^{15}N) and 72 ppm (^{13}C) sweep widths] experiments measured with 8 and 16 scans, respectively. Backbone resonances of residues E46, K74, G75, S96 and S119-Y123 were not observed in the spectrum and therefore were unassigned. Since the binding pocket residues exhibited slow exchange in the SPOP^{MATH}-Puc (1:5) complex, this spectrum was reassigned using three-dimensional HNCA, HNCO, HN(CA)CO and HNCACB experiments. For all of the three-dimensional experiments, the data were collected at 298K for samples containing 0.5 mM SPOP^{MATH} in NMR buffer. The positions of the resonances in the binding pocket that were in slow exchange in SPOP^{MATH}-Gli3$^{1\text{-}90}$ (1:2) and SPOP^{MATH}-SBM2 (1:4) complexes were very close to that of SPOP^{MATH}-pPuc complex and therefore were assigned as for the SPOP^{MATH}-pPuc complex.

Data were processed using Bruker Topspin version 3.2 and NMRPipe (v.7.9) [75] and were analyzed using CARA (v.1.8.4) [76].

^{1}H-^{15}N Transverse relaxation optimized spectroscopy–HSQC spectra of 350 μM ^{15}N SPOP^{MATH} in NMR buffer with increasing concentrations of Gli3$^{1\text{-}90}$ (to molar ratios of 1:1.75) were collected with 1024 (^{1}H) × 90 (^{15}N) complex data points and 32 scans with 12 ppm and 29 ppm for ^{1}H and ^{15}N sweep widths, respectively. Similar spectra were recorded for the complexes in the presence of different peptides, with protein/peptide molar ratios of 1:5 for Puc, 1:8 for Gli3$^{16\text{–}30}$, 1:4 for SBM2 and 1:4 for SBM3.

Gradient-selected sensitivity-enhanced ^{1}H-^{15}N HSQC spectra of 400 μM ^{15}N Gli3$^{1\text{-}90}$ in NMR buffer with increasing concentrations of SPOP^{MATH} (to molar ratios of 1:3) were recorded with 1024 × 150 complex data points and 16 scans. Intensity ratios for each resonance were calculated from the intensities in the free state and from intensities at increasing molar ratios at the same resonance frequencies to combine chemical shift perturbations and broadening into a single parameter of intensity loss.

hetNOEs were collected with a 2-s relaxation delay and with and without a 5-s presaturation delay, using 1024 × 200 complex data points and 32 scans with 10 ppm and 24 ppm for ^{1}H and ^{15}N sweep widths, respectively. The hetNOE values were calculated from the ratio of peak intensities of the saturated and unsaturated spectra. All the spectra were referenced directly using 4,4-dimethyl-4-silapentane-1-sulfonate for the ^{1}H dimension and ^{13}C and ^{15}N frequencies were referenced indirectly.

Secondary structural propensities were calculated by using $^{13}C^{\alpha}$ and $^{13}C^{\beta}$ chemical shifts using the SSP program [53].

Analytical ultracentrifugation

SV experiments of all protein samples were conducted in a ProteomeLab XL-I analytical ultracentrifuge (Beckman Coulter, Indianapolis, IN) following standard protocols unless mentioned otherwise [57,77]. A mixture of Gli3$^{1\text{-}90}$ (156 μM)/SPOP^{MATH} (525 μM), and a dilution series thereof, in the ultracentrifugation buffer (100 mM NaCl, 2.7 mM KCl, 10 mM Na_2HPO_4, 1.76 mM KH_2PO_4 and 5 mM DTT at pH 6.0), were loaded into a cell assembly composed of a double-sector charcoal-filled centerpiece with a 12-mm pathlength and sapphire windows. The cell assembly, containing identical sample and reference buffer volumes of 400 μL, was placed in a rotor and temperature equilibrated at rest at 20°C for 2 h before it was accelerated from 0 to 50,000 rpm. Rayleigh interference optical data were collected continuously for 10 h. The velocity data were modeled with diffusion-deconvoluted sedimentation coefficient distributions $c(s)$ in SEDFIT[‡], using algebraic noise decomposition and with the signal-average frictional ratio and meniscus position refined with non-linear regression. Maximum entropy regularization was applied at a confidence level of P=0.70. A two-dimensional size-and-shape distribution model, $c(s,f/f_0)$ (with the one dimension the s distribution and the other one the f/f_0 distribution) was also calculated with the same interference fringe displaced velocity data. The equidistant f/f_0 grid was from 1.0 to 3.0 with 0.13 steps, the linear s grid was from 0.5 to 5 S with 100 s-values, and Tikhonov–Phillips regularization at one standard deviation was applied. The data were transformed to a $c(M,f/f_0)$ contour distribution plot with M the molecular mass and f/f_0 the frictional ratio. The dotted lines indicate lines of constant s-value. The distributions were not normalized [57,78].

Biolayer interferometry

Binding affinities of Gli3$^{1\text{-}90}$ to SPOP^{MATH}, SPOP-$^{MATH\text{-}BTB}$ and SPOP$^{MATH\text{-}BTB\text{-}BACK}$ were measured by BLI using an OctetRED instrument (ForteBio). All proteins used for BLI were buffer exchanged with 20 mM Hepes, 150 mM NaCl, 5 mM DTT and 0.005% Tween 20 (pH 7.4). N-terminal His$_6$-Gli3$^{1\text{-}90}$ (0.1 μM) was immobilized on Ni-NTA biosensor (ForteBio) for 300 s. For baseline and surface stability, the captured His$_6$-Gli3$^{1\text{-}90}$ was

cross-linked for 60 s with a mixture of 0.1 M ethyl(dimethylaminopropyl) carbodiimide and 0.025 M *N*-hydroxysuccinimide and was subsequently quenched with 1 M ethanolamine for 60 s. Biosensors with immobilized His_6-$Gli3^{1-90}$ were subsequently dipped into different concentrations of SPOP samples for association until the signal reached a plateau. The SPOP samples used for BLI were produced from GST-tagged constructs to prevent Ni-mediated immobilization of SPOP on the biosensor. Binding of $SPOP^{MATH-BTB-BACK}$ was performed at concentrations 0, 0.01, 0.05, 0.1, 0.5, 1, 2.5 and 5 μM, and binding of $SPOP^{MATH-BTB}$ and $SPOP^{MATH}$ was performed at concentrations 0, 0.1, 0.5, 1, 2.5, 5, 10 and 20 μM. The concentrations of SPOP constructs with different valency were normalized to the number of protomers in solution; that is, solutions of 1 μM monomeric, dimeric and oligomeric SPOP contained the same number of binding sites for SB motifs. Dissociation of SPOP was monitored by subsequently incubating the biosensors in the buffer (20 mM Hepes, 150 mM NaCl, 5 mM DTT and 0.005% Tween 20 at pH 7.4). The sensorgram at each SPOP concentration was background subtracted using a reference sensorgram (obtained from biosensors without immobilized $Gli3^{1-90}$). The dissociation constants were obtained by fitting the data to a kinetic model for one-site binding.

In vitro ubiquitination assay

$Gli3^{1-90}$ ubiquitination was sampled in 50 mM Tris (pH 7.5), 150 mM NaCl, 10 mM $MgCl_2$, 5 mM ATP, 1 mM DTT and 2 mg/mL bovine serum albumin at room temperature at time points from 0 to 20 min. The reaction mixture contained ubiquitinating enzymes at final concentrations of 0.25 μM UBA1 (E1; in assays with lysine-less ubiquitin 1 μM UBA1 to reach maximum ubiquitination more rapidly), 5 μM UbcH5B (E2), 5 μM NEDD8-CUL3-Rbx1 (E3), 5 μM SPOP (either $SPOP^{MATH-BTB-BACK}$ or $SPOP^{MATH-BTB}$ as substrate adaptor), 75 μM ubiquitin or a lysine-less ubiquitin mutant (both BostonBiochem) and 5 μM His_6-tagged $Gli3^{1-90}$ or mutant versions. E1, E2 and E3 were purified as described previously [79,80,16]. The substrate and products were visualized by Western blot with anti-His antibody. The mutant versions of $Gli3^{1-90}$ were obtained by site-directed mutagenesis by replacing the Ser/Thr-rich regions with the generic disordered sequence GGSGS.

Mass spectrometry analysis of ubiquitination patterns

Ubiquitination reactions were run on an SDS-PAGE gel, and proteins in each lane were excised and reduced with DTT to break disulfide bonds and Cys residues were alkylated by iodoacetamide to allow the recovery of Cys-containing peptides. The gel bands were washed, dried in a vacuum concentrator and rehydrated with a buffer containing trypsin. Samples were digested overnight and the peptides were extracted using acetonitrile. The extracts were dried and each sample was then resuspended in 5% formic acid. For mass spectrometry analysis, the dried peptides were analyzed on an Orbitrap Fusion Tribrid mass spectrometer (Thermo Fisher Scientific) after separation on a 40 cm × 75 μm ID column packed with 1.9 μm C18 resin (Dr. Maisch GmbH, Germany). Separation was achieved by applying 10–40% buffer B gradient in 2 h (buffer A: 0.2% formic acid; buffer B: buffer A plus 70% ACN). The column was heated at 65°C by a butterfly portfolio heater (Phoenix S&T) to reduce backpressure. The mass spectrometer was operated in data-dependent and targeted mode with a survey scan in Orbitrap (60,000 resolutions, 2×10^5 AGC target and 50 ms maximal ion time). During data dependent acquisition, Orbitrap survey spectra were scheduled for execution at least every 3 s, with the embedded control system determining the number of MS/MS acquisitions executed during this period. A list of masses corresponding to all putative lysine modification sites of the $Gli3^{1-90}$ variants was used for targeted MS/MS acquisition to increase the sensitivity of detection. The parameters for MS/MS scans were HCD, 1×10^5 AGC target, 128 ms maximal ion time, 0.4 *m*/*z* isolation window, 38 normalized collision energy and 20 s dynamic exclusion. MS/MS raw files were converted into mzXML format and searched against UniProt mouse database populated with user--added protein sequences representing the mutated proteins by JUMP algorithm [81], a tag-based database search program.

Accession numbers

The backbone chemical shift assignments of $SPOP^{MATH}$, $SPOP^{MATH}$ + pPuc and $Gli3^{1-90}$ were deposited in the Biological Magnetic Resonance Bank database with the following IDs: 26629, 26631 and 26575, respectively.

Acknowledgements

We thank Jill Bouchard for technical help. This work was supported by R01GM112846-01 and a V Foundation Scholar Award (to T.M.), the National Cancer Institute Cancer Center Support Grant P30CA21765 (at St. Jude Children's Research Hospital), HHMI (to B.A.S.) and the American Lebanese Syrian Associated Charities.

Author Contributions: W.K.P., M.R.M., B.S. and T.M. designed the research; W.K.P., G.R., J.L., A.N., M.R.M., E.W. and A.A.H. performed the research; W.K.P., G.R., A.N., M.R.M., A.A.H., J.P. and T.M. analyzed data; W.K.P. and T.M. wrote the paper; and all authors edited the paper.

Conflict of Interest: The authors declare no conflict of interest.

Appendix A. Supplementary data

Supplementary data to this article can be found online at http://dx.doi.org/10.1016/j.jmb.2015.10.002.

Received 9 May 2015;
Received in revised form 5 October 2015;
Accepted 5 October 2015
Available online 22 October 2015

Keywords:
multivalency;
cancer;
degron;
Speckle-type POZ protein;
NMR spectroscopy

Present address: W. K. Pierce, Department of Chemical Biology and Therapeutics, St. Jude Children's Research Hospital, 262 Danny Thomas Place, Memphis, TN 38105, USA.

†see www.cBioPortal.org.
‡https://sedfitsedphat.nibib.nih.gov/software/default.aspx.

Abbreviations used:
AUC, analytical ultracentrifugation; β-ME, β-mercaptoethanol; BLI, biolayer interferometry; FA, fluorescence anisotropy; hetNOE, heteronuclear nuclear Overhauser enhancement; HSQC, heteronuclear single quantum coherence; MS/MS, tandem mass spectrometry; SB, SPOP binding; SV, sedimentation velocity; TEV, tobacco etch virus; wt, wild type.

References

[1] V. Neduva, R.B. Russell, Linear motifs: Evolutionary interaction switches, FEBS Lett. 579 (2005) 3342–3345.
[2] A. Mohan, C.J. Oldfield, P. Radivojac, V. Vacic, M.S. Cortese, A.K. Dunker, et al., Analysis of molecular recognition features (MoRFs), J. Mol. Biol. 362 (2006) 1043–1059.
[3] M. Fuxreiter, P. Tompa, I. Simon, Local structural disorder imparts plasticity on linear motifs, Bioinformatics 23 (2007) 950–956.
[4] N.E. Davey, G. Trave, T.J. Gibson, How viruses hijack cell regulation, Trends Biochem. Sci. 36 (2011) 159–169.
[5] R.J. Edwards, N.E. Davey, K. O'Brien, D.C. Shields, Interactome-wide prediction of short, disordered protein interaction motifs in humans, Mol. BioSyst. 8 (2012) 282–295.
[6] M. Buljan, G. Chalancon, A.K. Dunker, A. Bateman, S. Balaji, M. Fuxreiter, et al., Alternative splicing of intrinsically disordered regions and rewiring of protein interactions, Curr. Opin. Struct. Biol. 23 (2013) 443–450.
[7] P. Tompa, N.E. Davey, T.J. Gibson, M.M. Babu, A million peptide motifs for the molecular biologist, Mol. Cell 55 (2014) 161–169.
[8] P.E. Wright, H.J. Dyson, Intrinsically disordered proteins in cellular signalling and regulation, Nat. Rev. Mol. Cell Biol. 16 (2015) 18–29.
[9] U. Schwarz-Linek, E.S. Pilka, A.R. Pickford, J.H. Kim, M. Hook, I.D. Campbell, et al., High affinity streptococcal binding to human fibronectin requires specific recognition of sequential F1 modules, J. Biol. Chem. 279 (2004) 39017–39025.
[10] J. Hall, P.A. Karplus, E. Barbar, Multivalency in the assembly of intrinsically disordered Dynein intermediate chain, J. Biol. Chem. 284 (2009) 33115–33121.
[11] A. Sethi, B. Goldstein, S. Gnanakaran, Quantifying intramolecular binding in multivalent interactions: A structure-based synergistic study on Grb2-Sos1 complex, PLoS Comput. Biol. 7 (2011) e1002192.
[12] J.L. Morgan, Y. Song, E. Barbar, Structural dynamics and multiregion interactions in dynein-dynactin recognition, J. Biol. Chem. 286 (2011) 39349–39359.
[13] A. Nyarko, Y. Song, J. Novacek, L. Zidek, E. Barbar, Multiple recognition motifs in nucleoporin Nup159 provide a stable and rigid Nup159-Dyn2 assembly, J. Biol. Chem. 288 (2013) 2614–2622.
[14] M. Welcker, E.A. Larimore, J. Swanger, M.T. Bengoechea-Alonso, J.E. Grim, J. Ericsson, et al., Fbw7 dimerization determines the specificity and robustness of substrate degradation, Genes Dev. 27 (2013) 2531–2536.
[15] E. Barbar, A. Nyarko, Polybivalency and disordered proteins in ordering macromolecular assemblies, Semin. Cell Dev. Biol. 37 (2015) 20–25.
[16] W.J. Errington, M.Q. Khan, S.A. Bueler, J.L. Rubinstein, A. Chakrabartty, G.G. Prive, Adaptor protein self-assembly drives the control of a cullin-RING ubiquitin ligase, Structure 20 (2012) 1141–1153.
[17] T. Ravid, M. Hochstrasser, Diversity of degradation signals in the ubiquitin-proteasome system, Nat. Rev. Mol. Cell Biol. 9 (2008) 679–690.
[18] X. Tang, S. Orlicky, T. Mittag, V. Csizmok, T. Pawson, J.D. Forman-Kay, et al., Composite low affinity interactions dictate recognition of the cyclin-dependent kinase inhibitor Sic1 by the SCFCdc4 ubiquitin ligase, Proc. Natl. Acad. Sci. U. S. A. 109 (2012) 3287–3292.
[19] P. Nash, X. Tang, S. Orlicky, Q. Chen, F.B. Gertler, M.D. Mendenhall, et al., Multisite phosphorylation of a CDK inhibitor sets a threshold for the onset of DNA replication, Nature 414 (2001) 514–521.
[20] V.P. Ronchi, J.M. Klein, D.J. Edwards, A.L. Haas, The active form of E6-associated protein (E6AP)/UBE3A ubiquitin ligase is an oligomer, J. Biol. Chem. 289 (2014) 1033–1048.
[21] A. Kentsis, R.E. Gordon, K.L. Borden, Self-assembly properties of a model RING domain, Proc. Natl. Acad. Sci. U. S. A. 99 (2002) 667–672.
[22] M. McMahon, N. Thomas, K. Itoh, M. Yamamoto, J.D. Hayes, Dimerization of substrate adaptors can facilitate cullin-mediated ubiquitylation of proteins by a "tethering" mechanism: A two-site interaction model for the Nrf2-Keap1 complex, J. Biol. Chem. 281 (2006) 24756–24768.
[23] Q. Yin, S.C. Lin, B. Lamothe, M. Lu, Y.C. Lo, G. Hura, et al., E2 interaction and dimerization in the crystal structure of TRAF6, Nat. Struct. Mol. Biol. 16 (2009) 658–666.
[24] P. Peschard, G. Kozlov, T. Lin, I.A. Mirza, A.M. Berghuis, S. Lipkowitz, et al., Structural basis for ubiquitin-mediated dimerization and activation of the ubiquitin protein ligase Cbl-b, Mol. Cell 27 (2007) 474–485.
[25] M. Welcker, B.E. Clurman, Fbw7/hCDC4 dimerization regulates its substrate interactions, Cell Div. 2 (2007) 7.
[26] M.V. Poyurovsky, C. Priest, A. Kentsis, K.L. Borden, Z.Q. Pan, N. Pavletich, et al., The Mdm2 RING domain C-terminus is required for supramolecular assembly and ubiquitin ligase activity, EMBO J. 26 (2007) 90–101.
[27] X. Tang, S. Orlicky, Z. Lin, A. Willems, D. Neculai, D. Ceccarelli, et al., Suprafacial orientation of the SCFCdc4

dimer accommodates multiple geometries for substrate ubiquitination, Cell 129 (2007) 1165–1176.
[28] I. Hernandez-Munoz, A.H. Lund, P. van der Stoop, E. Boutsma, I. Muijrers, E. Verhoeven, et al., Stable X chromosome inactivation involves the PRC1 Polycomb complex and requires histone MACROH2A1 and the CULLIN3/SPOP ubiquitin E3 ligase, Proc. Natl. Acad. Sci. U. S. A. 102 (2005) 7635–7640.
[29] J.E. Kwon, M. La, K.H. Oh, Y.M. Oh, G.R. Kim, J.H. Seol, et al., BTB domain-containing speckle-type POZ protein (SPOP) serves as an adaptor of Daxx for ubiquitination by Cul3-based ubiquitin ligase, J. Biol. Chem. 281 (2006) 12664–12672.
[30] Q. Zhang, L. Zhang, B. Wang, C.Y. Ou, C.T. Chien, J. Jiang, A hedgehog-induced BTB protein modulates hedgehog signaling by degrading Ci/Gli transcription factor, Dev. Cell 10 (2006) 719–729.
[31] J. Liu, M. Ghanim, L. Xue, C.D. Brown, I. Iossifov, C. Angeletti, et al., Analysis of *Drosophila* segmentation network identifies a JNK pathway factor overexpressed in kidney cancer, Science 323 (2009) 1218–1222.
[32] M. Zhuang, M.F. Calabrese, J. Liu, M.B. Waddell, A. Nourse, M. Hammel, et al., Structures of SPOP-substrate complexes: Insights into molecular architectures of BTB-Cul3 ubiquitin ligases, Mol. Cell 36 (2009) 39–50.
[33] L.K. van Geersdaele, M.A. Stead, C.M. Harrison, S.B. Carr, H.J. Close, G.O. Rosbrook, et al., Structural basis of high-order oligomerization of the cullin-3 adaptor SPOP, Acta Crystallogr., Sect. D: Biol. Crystallogr. 69 (2013) 1677–1684.
[34] Q. Zhang, Q. Shi, Y. Chen, T. Yue, S. Li, B. Wang, et al., Multiple Ser/Thr-rich degrons mediate the degradation of Ci/Gli by the Cul3-HIB/SPOP E3 ubiquitin ligase, Proc. Natl. Acad. Sci. U. S. A. 106 (2009) 21191–21196.
[35] C.E. Barbieri, S.C. Baca, M.S. Lawrence, F. Demichelis, M. Blattner, J.P. Theurillat, et al., Exome sequencing identifies recurrent SPOP, FOXA1 and MED12 mutations in prostate cancer, Nat. Genet. 44 (2012) 685–689.
[36] M. Le Gallo, A.J. O'Hara, M.L. Rudd, M.E. Urick, N.F. Hansen, N.J. O'Neil, et al., Exome sequencing of serous endometrial tumors identifies recurrent somatic mutations in chromatin-remodeling and ubiquitin ligase complex genes, Nat. Genet. 44 (2012) 1310–1315.
[37] G. Boysen, C.E. Barbieri, D. Prandi, M. Blattner, S.S. Chae, A. Dahija, et al., SPOP mutation leads to genomic instability in prostate cancer, Elife 4 (2015) e09207.
[38] C. Geng, B. He, L. Xu, C.E. Barbieri, V.K. Eedunuri, S.A. Chew, et al., Prostate cancer-associated mutations in speckle-type POZ protein (SPOP) regulate steroid receptor coactivator 3 protein turnover, Proc. Natl. Acad. Sci. U. S. A. 110 (2013) 6997–7002.
[39] J. An, C. Wang, Y. Deng, L. Yu, H. Huang, Destruction of full-length androgen receptor by wild-type SPOP, but not prostate-cancer-associated mutants, Cell Rep. 6 (2014) 657–669.
[40] M.S. Kim, E.M. Je, J.E. Oh, N.J. Yoo, S.H. Lee, Mutational and expressional analyses of SPOP, a candidate tumor suppressor gene, in prostate, gastric and colorectal cancers, APMIS 121 (2013) 626–633.
[41] T. Davoli, A.W. Xu, K.E. Mengwasser, L.M. Sack, J.C. Yoon, P.J. Park, et al., Cumulative haploinsufficiency and triplosensitivity drive aneuploidy patterns and shape the cancer genome, Cell 155 (2013) 948–962.
[42] G. Li, W. Ci, S. Karmakar, K. Chen, R. Dhar, Z. Fan, et al., SPOP promotes tumorigenesis by acting as a key regulatory hub in kidney cancer, Cancer Cell 25 (2014) 455–468.
[43] J.P. Theurillat, N.D. Udeshi, W.J. Errington, T. Svinkina, S.C. Baca, M. Pop, et al., Prostate cancer. Ubiquitylome analysis identifies dysregulation of effector substrates in SPOP-mutant prostate cancer, Science 346 (2014) 85–89.
[44] N.P. Pavletich, C.O. Pabo, Crystal structure of a five-finger GLI-DNA complex: New perspectives on zinc fingers, Science 261 (1993) 1701–1707.
[45] D. Eliezer, Biophysical characterization of intrinsically disordered proteins, Curr. Opin. Struct. Biol. 19 (2009) 23–30.
[46] H.J. Dyson, P.E. Wright, Nuclear magnetic resonance methods for elucidation of structure and dynamics in disordered states, Methods Enzymol. 339 (2001) 258–270.
[47] T. Mittag, J.D. Forman-Kay, Atomic-level characterization of disordered protein ensembles, Curr. Opin. Struct. Biol. 17 (2007) 3–14.
[48] O. Zhang, L.E. Kay, J.P. Olivier, J.D. Forman-Kay, Backbone ^{1}H and ^{15}N resonance assignments of the N-terminal SH3 domain of drk in folded and unfolded states using enhanced-sensitivity pulsed field gradient NMR techniques, J. Biomol. NMR 4 (1994) 845–858.
[49] J. Yao, H.J. Dyson, P.E. Wright, Chemical shift dispersion and secondary structure prediction in unfolded and partly folded proteins, FEBS Lett. 419 (1997) 285–289.
[50] R. Tsanev, K. Vanatalu, J. Jarvet, R. Tanner, K. Laur, P. Tiigimagi, et al., The transcriptional repressor domain of Gli3 is intrinsically disordered, PLoS One 8 (2013) e76972.
[51] L.E. Kay, D.A. Torchia, A. Bax, Backbone dynamics of proteins as studied by ^{15}N inverse detected heteronuclear NMR spectroscopy: Application to staphylococcal nuclease, Biochemistry 28 (1989) 8972–8979.
[52] N.A. Farrow, O. Zhang, J.D. Forman-Kay, L.E. Kay, Characterization of the backbone dynamics of folded and denatured states of an SH3 domain, Biochemistry 36 (1997) 2390–2402.
[53] J.A. Marsh, V.K. Singh, Z. Jia, J.D. Forman-Kay, Sensitivity of secondary structure propensities to sequence differences between alpha- and gamma-synuclein: Implications for fibrillation, Protein Sci. 15 (2006) 2795–2804.
[54] M.H. Roehrl, J.Y. Wang, G. Wagner, A general framework for development and data analysis of competitive high-throughput screens for small-molecule inhibitors of protein–protein interactions by fluorescence polarization, Biochemistry 43 (2004) 16056–16066.
[55] T. Mittag, S. Orlicky, W.Y. Choy, X. Tang, H. Lin, F. Sicheri, et al., Dynamic equilibrium engagement of a polyvalent ligand with a single-site receptor, Proc. Natl. Acad. Sci. U. S. A. 105 (2008) 17772–17777.
[56] Z. Bozoky, M. Krzeminski, R. Muhandiram, J.R. Birtley, A. Al-Zahrani, P.J. Thomas, et al., Regulatory R region of the CFTR chloride channel is a dynamic integrator of phospho-dependent intra- and intermolecular interactions, Proc. Natl. Acad. Sci. U. S. A. 110 (2013) E4427–E4436.
[57] H. Zhao, C.A. Brautigam, R. Ghirlando, P. Schuck, Overview of current methods in sedimentation velocity and sedimentation equilibrium analytical ultracentrifugation, Curr. Protoc. Protein Sci. Chapter 20 (2013) 12.
[58] C. Bohr, K. Hasselbalch, A. Krogh, Ueber einen in biologischer beziehung wichtigen Einfluss, den die kohlensäurespannung des blutes auf dessen sauerstoffbindung

übt, Skandinavisches Archiv. Für Physiologie 16 (1904) 402–412.
[59] J.P. Changeux, The feedback control mechanisms of biosynthetic L-threonine deaminase by L-isoleucine, Cold Spring Harb. Symp. Quant. Biol. 26 (1961) 313–318.
[60] J.C. Gerhart, A.B. Pardee, The enzymology of control by feedback inhibition, J. Biol. Chem. 237 (1962) 891–896.
[61] H.B. Kamadurai, Y. Qiu, A. Deng, J.S. Harrison, C. Macdonald, M. Actis, et al., Mechanism of ubiquitin ligation and lysine prioritization by a HECT E3, eLife 2 (2013) e00828.
[62] D.C. Scott, V.O. Sviderskiy, J.K. Monda, J.R. Lydeard, S.E. Cho, J.W. Harper, et al., Structure of a RING E3 trapped in action reveals ligation mechanism for the ubiquitin-like protein NEDD8, Cell 157 (2014) 1671–1684.
[63] N.G. Brown, R. VanderLinden, E.R. Watson, R. Qiao, C.R. Grace, M. Yamaguchi, et al., RING E3 mechanism for ubiquitin ligation to a disordered substrate visualized for human anaphase-promoting complex, Proc. Natl. Acad. Sci. U. S. A. 112 (2015) 5272–5279.
[64] G. Wu, G. Xu, B.A. Schulman, P.D. Jeffrey, J.W. Harper, N.P. Pavletich, Structure of a beta-TrCP1-Skp1-beta-catenin complex: Destruction motif binding and lysine specificity of the SCF(beta-TrCP1) ubiquitin ligase, Mol. Cell 11 (2003) 1445–1456.
[65] H. Wu, Higher-order assemblies in a new paradigm of signal transduction, Cell 153 (2013) 287–292.
[66] A.N. Nguyen Ba, B.J. Yeh, D. van Dyk, A.R. Davidson, B.J. Andrews, E.L. Weiss, et al., Proteome-wide discovery of evolutionary conserved sequences in disordered regions, Science Signal. 5 (2012) rs1.
[67] N.E. Davey, K. Van Roey, R.J. Weatheritt, G. Toedt, B. Uyar, B. Altenberg, et al., Attributes of short linear motifs, Mol. BioSyst. 8 (2012) 268–281.
[68] E. Cerami, J. Gao, U. Dogrusoz, B.E. Gross, S.O. Sumer, B.A. Aksoy, et al., The cBio cancer genomics portal: An open platform for exploring multidimensional cancer genomics data, Cancer Discov. 2 (2012) 401–404.
[69] J. Gao, B.A. Aksoy, U. Dogrusoz, G. Dresdner, B. Gross, S.O. Sumer, et al., Integrative analysis of complex cancer genomics and clinical profiles using the cBioPortal, Sci Signal. 6 (2013) pl1.
[70] M. Krauthammer, Y. Kong, B.H. Ha, P. Evans, A. Bacchiocchi, J.P. McCusker, et al., Exome sequencing identifies recurrent somatic RAC1 mutations in melanoma, Nat. Genet. 44 (2012) 1006–1014.
[71] Cancer Genome Atlas Research Network, C. Kandoth, N. Schultz, A.D. Cherniack, R. Akbani, Y. Liu, et al., Integrated genomic characterization of endometrial carcinoma, Nature 497 (2013) 67–73.
[72] M.C. Rodrigo-Brenni, D.O. Morgan, Sequential E2s drive polyubiquitin chain assembly on APC targets, Cell 130 (2007) 127–139.
[73] K. Wu, J. Kovacev, Z.Q. Pan, Priming and extending: A UbcH5/Cdc34 E2 handoff mechanism for polyubiquitination on a SCF substrate, Mol. Cell 37 (2010) 784–796.
[74] N.G. Brown, E.R. Watson, F. Weissmann, M.A. Jarvis, R. VanderLinden, C.R. Grace, et al., Mechanism of polyubiquitination by human anaphase-promoting complex: RING repurposing for ubiquitin chain assembly, Mol. Cell 56 (2014) 246–260.
[75] F. Delaglio, S. Grzesiek, G.W. Vuister, G. Zhu, J. Pfeifer, A. Bax, NMRPipe: A multidimensional spectral processing system based on UNIX pipes, J. Biomol. NMR 6 (1995) 277–293.
[76] R. Keller, The Computer Aided Resonance Assignment Tutorial, first ed. CANTINA Verlag, Switzerland, 2004.
[77] P. Schuck, Size-distribution analysis of macromolecules by sedimentation velocity ultracentrifugation and lamm equation modeling, Biophys. J. 78 (2000) 1606–1619.
[78] P.H. Brown, P. Schuck, Macromolecular size-and-shape distributions by sedimentation velocity analytical ultracentrifugation, Biophys. J. 90 (2006) 4651–4661.
[79] N. Zheng, B.A. Schulman, L. Song, J.J. Miller, P.D. Jeffrey, P. Wang, et al., Structure of the Cul1-Rbx1-Skp1-F boxSkp2 SCF ubiquitin ligase complex, Nature 416 (2002) 703–709.
[80] D.T. Huang, M. Zhuang, O. Ayrault, B.A. Schulman, Identification of conjugation specificity determinants unmasks vestigial preference for ubiquitin within the NEDD8 E2, Nat. Struct. Mol. Biol. 15 (2008) 280–287.
[81] X. Wang, Y. Li, Z. Wu, H. Wang, H. Tan, J. Peng, JUMP: A tag-based database search tool for peptide identification with high sensitivity and accuracy, Mol. Cell. Proteomics 13 (2014) 3663–3673.